Journal of Alloys and Compounds 509 (2011) 3493–3496

Contents lists available at ScienceDirect

Journal of Alloys and Compounds

journal homepage: www.elsevier.com/locate/jallcom

Novel metallic iron/manganese–zinc ferrite nanocomposites prepared by microwave hydrothermal flash synthesis

T. Caillot [a,*], G. Pourroy [b], D. Stuerga [c]

[a] Université Lyon1, CNRS, UMR 5256, IRCELYON, Institut de Recherches sur la Catalyse et l'Environnement de LYON, 2 Avenue Albert Einstein, 69626 Villeurbanne, France
[b] IPCMS, Institut de Physique et de Chimie des Matériaux de Strasbourg, 23 rue du Lœss, BP 43, 67034 Strasbourg Cedex 2, France
[c] Laboratoire Interdisciplinaire Carnot de Bourgogne (LICB), département Nanosciences, Groupe d'Etudes et de Recherches sur les Microondes (GERM), UMR 5209 CNRS-Université de Bourgogne, BP 47870, 21078 Dijon Cedex, France

ARTICLE INFO

Article history:
Received 13 October 2010
Accepted 14 December 2010
Available online 22 December 2010

Keywords:
Microwave
Hydrothermal synthesis
Nanocomposites
Metallic iron
Manganese–zinc ferrite

ABSTRACT

Metallic iron (α-Fe)/manganese–zinc ferrite ($Fe_{3-x-y}Mn_xZn_yO_4$) nanocomposites have been successfully synthesized for the first time using microwave hydrothermal treatment of alcoholic solutions of chloride precursors and sodium ethoxide. This new type of nanocomposites, never obtained by conventional synthesis, can now be produced in a short period (e.g. 15 s). The powders were characterized by X-ray diffraction, transmission electron microscopy and magnetic properties were measured. In most cases, three classes of crystallites were observed; one of them is composed of grains of about 100 nm in size where the metal is inserted into the oxide. For all samples, 20% of metallic iron was routinely obtained using the microwave flash synthesis. Consequently, the microwave heating appears to provide an efficient source of energy in producing metallic iron nanoparticles protected against oxidation by an oxide matrix.

1. Introduction

Manganese zinc ferrites are typical examples of soft ferrites which have become important to industry because of their magnetic and dielectric properties [1,2]. They are widely used in technology as materials for coil cores in microwave broadband components. Many physical properties of polycrystalline ferrites depend on their microstructure which, in turns, strongly depends on the preparation processes [3]. Various techniques have been used to synthesize these compounds: solid state reaction [4], co-precipitation process [5], hydrothermal route [6] and sol–gel method [7] can be found in the literature. Typical drawbacks of conventional preparation methods are phase inhomogeneity, various particle size distribution and poor magnetization properties when fine particles, with narrow size distribution, are desirable for producing ceramics with enhanced reliability. Microwave synthesis is an alternative way to produce inorganic compounds because microwave heating is an in situ mode of energy conversion very attractive for chemists [8–10]. Since 20 years, Stuerga et al. have designed an original monomode microwave reactor called the RAMO system (french acronym of Reacteur Autoclave MicroOnde) [11–13]. This device is able to produce rapid bulk heating and to raise temperature of ethanol from ambient to 160 °C in 15 s (pressure is ~1 MPa and heating rate is close to ten degrees per second) [14]. RAMO system has allowed production of various nanomaterials [15–20]. In particular, metal/ferrites nanocomposites were obtained by disproportionation in an alcoholic medium of iron ethoxide into metallic iron and magnetite [21]. Insertion of metallic iron in manganese zinc ferrite could improve magnetization of manganese zinc ferrites samples. In the same spirit, this paper presents the first attempt to adapt the microwave one-step flash synthesis for the production of metallic iron/manganese–zinc ferrite nanocomposites.

2. Experimental

Nanocomposites were synthesized according to the protocol described in previous study [14]. All the chemicals reactants, $FeCl_2{\cdot}4H_2O$ (Prolabo, Normapur), $MnCl_2{\cdot}4H_2O$ (Prolabo, Normapur), $ZnCl_2$ (Prolabo, Normapur), sodium ethoxide (EtONa, Aldrich, 96%) and ethanol (Prolabo, Normapur, 96%) were reagents grade, and then, used without further purification. Ethanol and sodium ethoxide were employed to achieve concomitant olation and oxolation reactions [20]. Concentrations were chosen according to results obtained in previous studies [14,21]. Consequently, the iron salt concentration was fixed at 0.2 M, the manganese salt concentration at 0.025 M, the sodium ethoxide concentration at 1 M and various concentrations were tested for zinc salt. The reactants have been treated by microwave induced thermal hydrolysis with RAMO system. Different heating times (from 15 s to 10 min) were tested. After this thermal treatment, the as-synthesized powders were centrifuged and washed with distilled water in order to eliminate sodium and chloride ions. Finally, they were lyophilizing in order to remove any remaining solvent and prevent agglomeration of particles.

XRD measurements were performed at room temperature using a D5000 Siemens diffractometer equipped with a monochromatic beam Cu K_β ($\lambda = 0.139$ nm) focused with a secondary curved graphite monochromator. Patterns were collected

* Corresponding author. Tel.: +33 4 72 44 58 58; fax: +33 4 72 44 53 99.
E-mail address: thierry.caillot@ircelyon.univ-lyon1.fr (T. Caillot).

0925-8388/$ – see front matter © 2010 Elsevier B.V. All rights reserved.
doi:10.1016/j.jallcom.2010.12.096

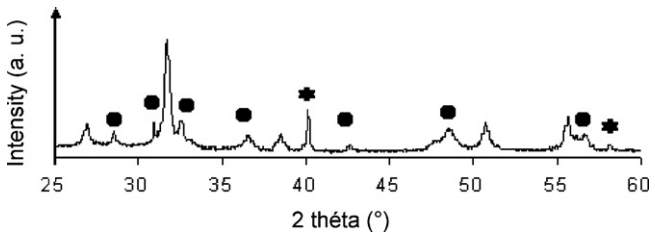

Fig. 1. X-ray diffraction patterns of samples produced from [EtONa] = 1 M, $[Fe^{2+}]$ = 0.2 M, $[Mn^{2+}]$ = 0.025 M and $[Zn^{2+}]$ = 0.05. The *correspond to metallic iron diffraction lines and the • to zinc oxide diffraction lines. The other diffraction lines correspond to the spinel phase.

in the 25–60 2θ range with a step increment of 0.03 and 100 s of counting time. Rietveld refinements [22] by using the XND program developed by Bérar [23,24] permitted to estimate the percentage of each phase. High resolution transmission electron microscopy (HRTEM) fitted with an energy-dispersive X-ray spectroscopy (EDSX) system was used to gather microstructural information about the as-produced powders. The individual grain compositions and the phase distribution within particles were investigated by selected area electron diffraction (SAED) and dark field imaging. The powders were embedding into an Epon 812 resin and then cut thin slices using an ultramicrotome equipped with a diamond knife. The 60–90 nm thick sections were then collected on a holey, carbon coated, 200 mesh copper grid. The samples were examined with a TOPCON 002B microscope operating at 200 kV (point to point resolution of 0.18 nm) and equipped with an ultrathin window KEVEX EDX spectrometer.

Metallic iron and manganese zinc ferrite present magnetic properties. The irreversibility of magnetization mechanisms is traduced by a hysteresis cycle. In this study, the hysteresis cycles of the composite were recorded at room temperature with a Foner type apparatus EG&G 155.

3. Results and discussion

The iron salt concentration was fixed at 0.2 M, the manganese salt concentration at 0.025 M, the sodium ethoxide concentration at 1 M while various concentrations were tested for zinc salt. Depending on zinc chloride concentration, XRD analysis showed different profiles:

- For $[Zn^{2+}] > 0.025$ M, metallic iron and manganese–zinc ferrite were present but small quantities of zinc oxide (ZnO) were also detected whatever the holding time was (see Fig. 1).

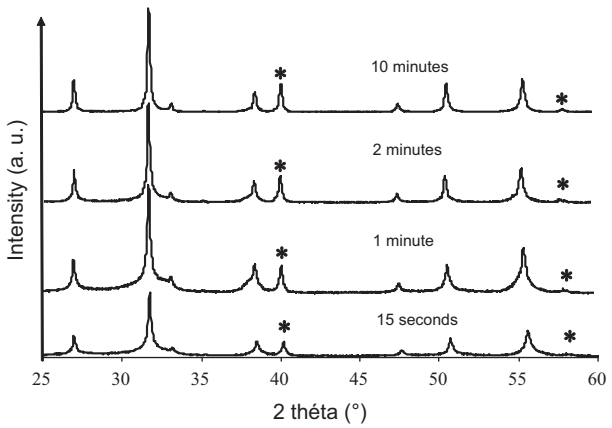

Fig. 2. X-ray diffraction patterns of Fe/manganese–zinc ferrite produced from [EtONa] = 1 M, $[Fe^{2+}]$ = 0.2 M, $[Mn^{2+}]$ = 0.025 M and $[Zn^{2+}]$ = 0.025. The *correspond to metallic iron diffraction lines. The other diffraction lines correspond to the spinel phase.

- For $[Zn^{2+}] \leq 0.025$ M, metallic iron and manganese-zinc ferrite were obtained without any other phase.

A study versus the heating time was also done for $[Zn^{2+}]$ = 0.025 M. Fig. 2 displays the XRD patterns obtained after different holding time (15 s to 10 min). All the samples showed well-defined X-ray diffraction patterns with very low backgrounds indicating a good crystallization since no final heat treatment was carried out on powder. They exhibited a spinel phase $Fe_{2+y}Mn_{1-x-y}Zn_xO_4$ and a metallic phase Fe^0. This mixture was never obtained by conventional synthesis in boiling KOH [25–27] mainly due to the systematic presence of large quantities of zinc oxide (ZnO).

Small quantities of akaganeïte (β-FeOOH) or hematite (α-Fe_2O_3) were detected for all conditions. When mixing was carried out under inert atmosphere, these spurious phases were not detected. These impurities were also formed by oxidation of ferrous ions by ambient oxygen of air during mixing of the two solutions.

The morphology of the as-produced powders has been investigated in details using transmission electron microscopy. Three

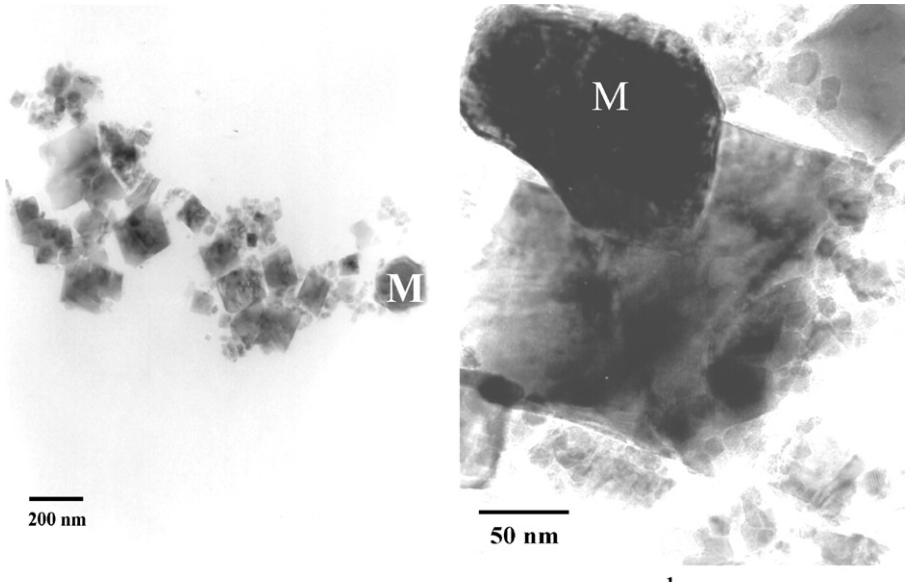

Fig. 3. TEM micrographs for $[Fe^{2+}]$ = 0.2 M, $[Mn^{2+}]$ = 0.025 M, $[Zn^{2+}]$ = 0.025 M and [EtONa] = 1 M treated 10 s (a) and treated 10 min (b). M correspond to the crystals which contains metallic iron.

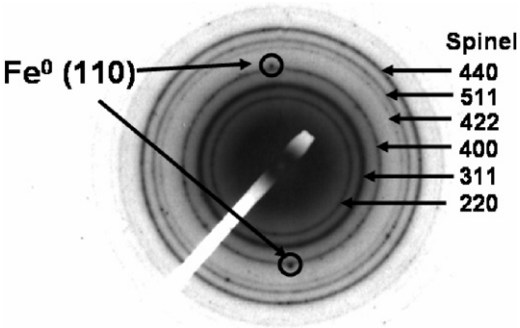

Fig. 4. Diffraction pattern performed of the grains of Fig. 3b.

classes of crystallites were observed whatever the heating duration was (Fig. 3):

(1) Elementary spherical grains with a diameter close to 10 nm.
(2) Particles in form of lozenge with a size between 50 and 200 nm.
(3) Grains without particular form with a size between 50 and 200 nm marked M.

The EDSX analysis indicated a large percentage of iron, manganese, zinc and oxygen in all particles. Nevertheless, this measurement has not allowed us to distinguish the spinel phase from metallic iron. Phase composition of different grain types was determined by SAED on diffraction pattern (Fig. 4) and dark field imaging. Crystallites (1) and (2) corresponded to manganese–zinc ferrite phase only when grains (3) were composed of metallic iron (white parts)/manganese–zinc ferrite (black parts) (Fig. 5). These particles presented a composite structure.

The formation of spinel phase crystallites (1) and (2) can be explained by an oxidation process. Indeed, when the two solutions are mixed, the precipitate of $Fe(OEt)_2$ obtained is most likely partially oxidized in $Fe(OEt)_3$ by oxygen of air or by small amounts of water present in ethanol. The manganese zinc ferrite $Fe_{2+y}Mn_{1-x-y}Zn_xO_4$ is produced via hydrolysis and condensation due to presence of $Mn(OEt)_2$, $Zn(OEt)_2$, $Fe(OEt)_2$ and $Fe(OEt)_3$ in solution as described by:

$$1-x-yMn(OEt)_2 + xZn(OEt)_2 + 2Fe(OEt)_3 + yFe(OEt)_2 + 4H_2O \rightarrow Fe_{2+y}Mn_{1-x-y}Zn_xO_4 + 8EtOH \quad (1)$$

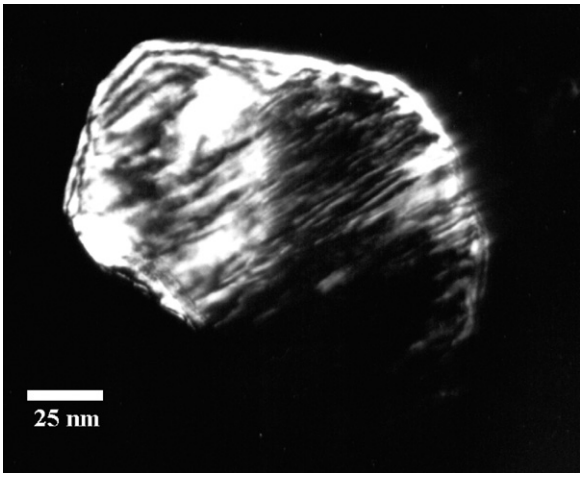

Fig. 5. TEM dark field micrograph of metallic iron/manganese–zinc ferrite synthesized from $[Fe^{2+}] = 0.2$ M, $[Mn^{2+}] = 0.025$ M, $[Zn^{2+}] = 0.025$ M and $[EtO^-] = 1$ M treated 10 min. White parts correspond to metallic iron and black parts to manganese–zinc ferrite.

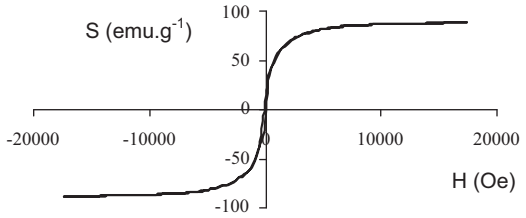

Fig. 6. Hysteresis cycle recorded at 300 K on the sample $[Fe^{2+}] = 0.2$ M, $[Mn^{2+}] = 0.025$ M, $[Zn^{2+}] = 0.025$ M and [EtONa] = 1 M treated 10 min.

According to previous investigations [14], hydrolysis and condensation generated two classes of crystallite: one produced at ambient temperature (1) when the second is formed during microwave heating (2).

The formation of composite crystallites (3) is most likely related to the disproportionation of $Fe(OEt)_2$ [14,21] under microwaves in an alcoholic media following by hydrolysis and condensation processes (1). Then, the disproportionation reaction is:

$$3Fe(OEt)_2 \rightarrow 2Fe(OEt)_3 + Fe^0 \quad (2)$$

A competition between dismutation process under microwave heating and oxidation process at ambient temperature and under microwaves has also occurred in the reactor during synthesis process.

The amount of each phase for the samples was difficult to measure using TEM because of the presence of biphasic particles. In addition, presence of adsorbed water leads to an underestimated amount of metallic iron through thermogravimetric route. Anyway, a first estimation using Rietveld refinements on XRD patterns gave a metallic phase percentage close to 20% whatever the holding time was. It is important to note that XRD patterns and metallic iron proportion do not vary after long duration storage and remains identical after two years in air in a pill-box. This result demonstrated clearly that metallic iron particles in nanocomposite structure do not suffer from ambient air oxidation.

In order to compare properties of nanocomposites with traditional manganese zinc ferrites, the samples were characterized by magnetic measurements. Fig. 6 presents the hysteresis cycle recorded at 300 K for a sample heat treated 10 min. The magnetization was completely saturated for a Field of 8000 Oe with a saturation magnetization (S) in the range of 90 emu g^{-1} for all the powders. These results indicated a higher magnetization obtained for a lower field compared to manganese–zinc ferrite nanoparticles (60 emu g^{-1}) produced by conventional methods [28–30]. These results suggest that metallic iron enhance magnetization of nanocomposite powders as expected. On the contrary, coercive field was very low (50–80 Oe). A comparison with powders obtained by other synthesis process was impossible because these nanocomposites were never obtained by other synthesis modes to our knowledge. However, the nanometric grain size and the microstructure could most likely explain these low coercive field values.

4. Conclusion

For specific operating conditions, the microwave-heating of alcoholic ferrous chloride solutions with sodium ethoxide can lead in a very short time (a few minutes) to metallic iron/manganese–zinc ferrite nanocomposites. The RAMO system combines the iron (II) disproportionation with very fast heating rate of microwave to obtain these compounds. Conventional hydrothermal treatments of the same solutions cannot produce such nanocomposites. It is difficult to explain why the microwave heating drives the reaction along a different pathway compared

to the conventional heating. Further work is required to improve understanding of the process and the characterization of the nanocomposites produced.

Acknowledgements

The author wish to express their thanks to Dr. D. Charriere and Dr. C. Gras for fruitful discussion and encouragement's.

References

[1] A. Goldman, Handbook of Ferromagnetic Materials, Kluwer Academic Publishers, Boston, 1999.
[2] E.P. Wolfarth, Ferromagnetic Materials—A Handbook on the Properties of Magnetically Ordered Substances, vol. 2, Elsevier, Amsterdam, 1986.
[3] M.A. El Hiti, A.I. El Shora, S.M. Hammad, Mater. Sci. Technol. 13 (1997) 625–630.
[4] T. Ogasawara, L.M. Tavares, S.S. Marins, Mater. Lett. 61 (2007) 5063–5066.
[5] B. Jeyadevan, K. Tohji, K. Nakatsuka, A. Narayanasamy, J. Magn. Magn. Mater. 217 (2000) 99–105.
[6] Q. Zhang, M. Zhu, Q. Zhang, Y. Li, H. Wang, J. Magn. Magn. Mater. 321 (2009) 3203–3206.
[7] L. Dong, Z. Han, Y. Zhang, Z. Wu, X. Zhang, J. Rare Earths 24 (2006) 54–56.
[8] S. Komarneni, M.C. D'arrigo, C. Leonelli, G.C. Pellacani, H. Katsuki, J. Am. Ceram. Soc. 81 (1998) 3041–3043.
[9] S. Komarneni, V.C. Menon, Mater. Lett. 27 (1996) 313–315.
[10] M. Park, S. Komarneni, R. Roy, Mater. Lett. 43 (2000) 359–363.
[11] D. Stuerga, T. Caillot, in: J. Takadoum (Ed.), Nanomaterials and Surface Engineering, Wiley-ISTE, 2010, pp. 163–206, Chapter 6.
[12] D. Stuerga, in: A. Loupy (Ed.), Microwaves in Organic Synthesis 2, Wiley-VCH, Weinheim, 2006, pp. 1–61, Chapter 1.
[13] B. Ondruschka, W. Bonrath, D. Stuerga, in: A. Loupy (Ed.), Microwaves in Organic Synthesis 2, Wiley-VCH, Weinheim, 2006, pp. 62–107, Chapter 2.
[14] T. Caillot, G. Pourroy, D. Stuerga, J. Solid State Chem. 177 (2004) 3843–3848.
[15] K. Bellon, D. Chaumont, D. Stuerga, J. Mater. Res. 16 (2001) 2619–2622.
[16] E. Michel, D. Stuerga, D. Chaumont, J. Mater. Sci. Lett. 20 (2001) 1593–1595.
[17] J.C. Niepce, D. Stuerga, T. Caillot, J.P. Clerk, A. Granovsky, M. Inoue, N. Perov, G. Pourroy, A. Radkovskaya, IEEE Trans. Magn. 38 (2002) 2622–2624.
[18] L. Combemale, G. Caboche, D. Stuerga, D. Chaumont, Mater. Res. Bull. 40 (2005) 529–536.
[19] L. Combemale, G. Caboche, D. Stuerga, J. Solid State Chem. 182 (2009) 2829–2834.
[20] C. Bousquet-Berthelin, D. Stuerga, J. Mater. Sci. 40 (2005) 253–255.
[21] T. Caillot, D. Aymes, D. Stuerga, N. Viart, G. Pourroy, J. Mater. Sci. 37 (2002) 5153–5158.
[22] H.M. Rietveld, J. Appl. Crystallogr. 2 (1969) 65–71.
[23] J.F. Bérar, P. Lelann, J. Appl. Crystallogr. 24 (1991) 1–5.
[24] J.F. Bérar, G. Baldinozzi, IUCR-CP Newslett. 20 (1998) 3–5.
[25] J.C. Yamegni-Noubeyo, G. Pourroy, J. Werckmann, A. Malats i Riera, G. Ehret, P. Poix, J. Am. Ceram. Soc. 79 (1996) 259–270.
[26] G. Pourroy, A. Vallez-Minguez, T. Dintzer, M. Richard-Plouet, J. Alloys Compd. 327 (2001) 267–269.
[27] G. Pourroy, S. Läkamp, S. Vilminot, J. Alloys Compd. 244 (1996) 90–93.
[28] B. Skolyszewska, W. Tokarz, K. Prybylski, Z. Kakol, Physica C 387 (2003) 290–294.
[29] P. Poddar, H. Srikanth, S.A. Morrison, E.E. Carpenter, J. Magn. Magn. Mater. 288 (2005) 443–451.
[30] S. Son, R. Swaminathan, M.E. McHenry, J. Appl. Phys. 93 (2003) 7495–7497.